Journal of Robotics and Control (JRC)
Volume 6, Issue 3, 2025
ISSN: 2715-5072, DOI: 10.18196/jrc.v6i3.25848 

# Development of a Flexure Based Mechanism for Robotic Micro-Surgical Applications

Muhammed Gaafar [1*], Abdullah T. Elgammal [2], Ahmed El-Betar [3], Mahmoud Magdy [4]
[1, 3, 4] Mechanical Engineering Department, Benha University, Benha, Egypt.
[2] Electrical Engineering Department, Benha University, Benha, Egypt.
[2, 4] Mechanical Engineering Department, The British University inEgypt (BUE), Cairo, Egypt.
Email: [1] gaafar@bhit.bu.edu.eg, [2] abdalla.elgammal@bhit.bu.edu.eg,
[3] ahmed.elbetar@bhit.bu.edu.eg, [4] mahmoud.mohamed@bue.edu.eg
*Corresponding Author

***Abstract*—Traditional robot-assisted surgery, which relies on conventional mechanical mechanisms, has certain drawbacks, including friction, backlash, and the need for lubricants. In contrast, compliant mechanisms utilizing flexure joints can achieve the desired motion while minimizing the disadvantages associated with movable joints. This research introduces a novel approach to address the issues prevalent in robot-assisted surgery. Our device incorporates flexure joints to enhance movement and eliminate complications posed by traditional movable joints. The primary focus of this study is on designing, analyzing, and validating a flexible remote center-of-motion (RCM) mechanism intended for robot-assisted surgery. SolidWorks was used for modeling of the proposed mechanism with different configurations of joints arrangement, and finite element analysis (FEA) was performed using ANSYS to evaluate and compare different design iterations in terms of RCM point drift in X and Y axis. Experimental Results show that the optimized design keeps the RCM point drift within acceptable microsurgical limits, with measured displacements of 1.02 $mm$ along the x-axis and 2.07 $mm$ along the y-axis. These results highlight the potential of compliant mechanism to improve the accuracy and safety of robot-assisted microsurgical procedures and point to a significant improvement over current mechanism.**

***Keywords*—Flexure-Based Mechanisms; Finite Element Modeling in Surgical Robots; 3D Printed Surgical Robots**

## I. Introduction

Clinical practices often entail managing microscopic, complex structures. Alongside other organ systems, these structures are widely present in the nervous system, auditory system, visual system, and various components of the circulatory system [1]. Medical robotics is designed to extend surgeons' skills and enhance surgery results by offering versatile tools rather than replacing human expertise. In earlier work, miscellaneous clinical applications emerged by demonstrating new mechanisms, resulting in noteworthy developments in surgical robotics [2]–[14].

The progression of surgical assisting robots improves surgical outcomes, essential surgeon skills, operational efficiency, and patient satisfaction. One of the most critical challenges in this field is maintaining the surgical instrument's motion through a fixed point—the incision—without exerting force that could stretch or damage the surrounding tissue. This constraint ensures patient safety by preventing secondary injury, and it defines a fundamental design requirement for surgical robotic systems as discussed in [15]–[22]. To enforce this constraint, robotic arms must incorporate precise motion restrictions. While early approaches employed multi-joint linkage systems and passive joints, these methods were limited by external physiological influences like patient movement or breathing [23]. In contrast, mechanism-based constraints, particularly through the use of Remote Center of Motion (RCM) mechanisms, have emerged as the most reliable and robust solution [24].

The RCM mechanism is designed to ensure that part of a robot's structure moves through a virtual, fixed spatial point—typically the incision—without any physical joint or pivot located there. This property makes RCM mechanisms uniquely suited for minimally invasive surgery, where access is constrained and precision is critical. As such, the RCM mechanism has become the core structural principle of modern minimally invasive surgical robots, directly influencing their dexterity, precision, and clinical effectiveness [25]–[30].

Various RCM mechanism types have been developed, including arc-shaped , spherical , and double-parallelogram designs [31]. Each offers distinct advantages: arc-shaped mechanisms are compact and simple; spherical mechanisms enable multi-axis rotation with minimal interference; and double-parallelogram mechanisms, such as those used in the Da Vinci surgical robot, offer high precision and mechanical robustness [32]–[36].

The typical RCM mechanisms employed in surgical robots are composed of stiff body parts and mechanical joints, which can lead to defects, including clearance, backlash, hysteresis, and lubrication that interfere with system sterilization [25]–[30]. Nevertheless, a significant performance and design flexibility enhancement is achieved by shifting from conventional rigid-link RCM mechanisms to those utilising flexure joints

[37]–[42]. Flexure mechanisms, which achieve motion through elastic deformation of compliant elements, offer substantial advantages for surgical applications:

- Elimination of friction and backlash, leading to smoother, more precise movement.
- Miniaturization potential, essential for compact and lightweight robotic designs.
- High repeatability and low maintenance, as there are no sliding or rotating parts that wear over time.
- Intrinsic stiffness tuning, allowing designers to balance flexibility with structural stability.

The integration of flexure joints enhances the motion control of RCM-based surgical robots and aligns with the broader goals of improving patient outcomes, reducing surgical invasiveness, and expanding the accessibility of robot-assisted surgery across different medical disciplines. Complete design, dynamic simulation and experimental verification of RCM point drifting are needed to prove the feasibility of the proposed system. The planar RCM mechanism with cruciform and circular notch flexure joints is discussed in [43]–[47]. The major problem with compliant RCM mechanisms is point drifting. The essential analyses for compliant RCM mechanisms are kinematic and dynamic to checkpoint drifting. Nevertheless, none of the earlier research had such a significant analysis as their primary focus. The existing compliant RCM mechanism has limitations, such as the limited range of tilting angles and the large RCM point drift [48]–[51].

This research aims to build and validate a compliant RCM mechanism for the microsurgery application in a straightforward and compact structure. The proposed compliant RCM mechanism is merged with the rolling stage and positioner of 3 transitional motions in the three axes $x$, $y$, and $z$. The proposed compliant RCM mechanism can produce the tilting angle required for surgery; therefore, this study mainly focuses on tilting motion and minimizing the RCM point drift. Furthermore, an experimental environment was held to validate the point drift of the proposed system.

## II. Material and Methods

### A. System Description

The proposed system comprises an approaching stage, a rotational stage, and a tilting stage, as shown in Fig. 1. All these stages are designed for microsurgery. We exported the CAD model of the approaching and rotating stages, which were designed in SolidWorks, into ADAMS software to calculate the force and torque of every stage. The transitional axes $X$, $Y$, and $Z$ axes have a 50x50x50 $mm$ range. Moreover, the rotational stages support rotation motion in the range of ±30o, which is adequate for most micro-surgical applications. According to measurements reported, $95\%$ of all surgical tool motions during a typical microsurgery procedure are confined inside a zone defined by a cone with a vertex angle of 60 degrees corresponding to ($\pm 30^{\circ}$). When connected in parallel, parallelograms provide a 2-DOF RCM mechanism that encounters very general applications [52], [53]. Fig. 2 shows a primary setup of parallelogram-based RCM systems [54], [55]. We replaced the conventional parallelogram hinges with large deflection compliance flexures to implement the proposed RCM.

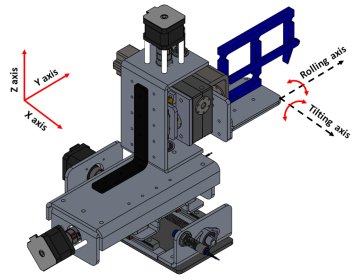


Fig. 1. 3D CAD model for the proposed system.

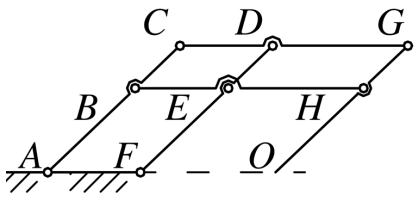


Fig. 2. RCM mechanism based on parallelogram [54].

The parasitic displacement of any particular flexure will influence the functioning of the remote centre of motion (RCM) mechanism. This results from the differing degrees of parasitic displacement and stiffness exhibited by each flexure. To resolve this, we utilised the Rigid Body Replacement (RBR) method for modelling the parallelograms that constitute the RCM mechanisms, enabling us to determine the ideal design for each mechanism [56]–[61]. This approach is based on classifying flexures into two joint groups: Group 1 corresponds to planar flexures, and Group 2 corresponds to spatial flexure joints. Based on references [45], [46], [62]–[64], the range of motion and axis drift of joints impact flexure joint performance. A study was conducted on high-performance spatial and planar flexure joints, extending previous research on their functionality as indicated in references [31], [43], [65]–[68]. We transmit the results for spatial joints with cruciform and split tube joints, which can provide extensive ranges of motion with an axis deviation very close to zero, and for the planar joints through circular and semi-circular undercut notches. The shape and dimensions of the flexures proposed are shown in Fig. 3.

Fig. 2 illustrates the proposal to substitute hinge joints A, F, C, D, and G with flexure joints A and B. We execute to substitute hinge joints B, E, and H with flexure joints C and D, as depicted in Figure 4.

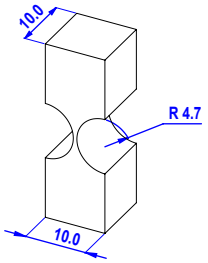


(a) Circular flexure (Joint A)

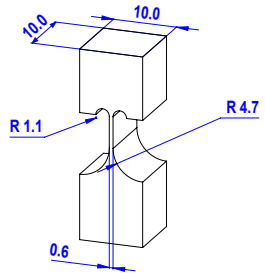


(b) Semi-circular undercut flexure (Joint B)

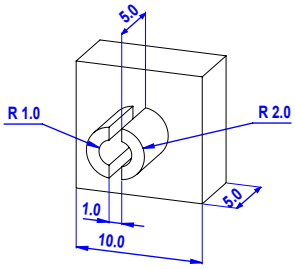


(c) Spilt tube flexure (Joint C)

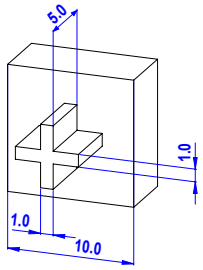


(d) Cruciform flexure (Joint D)

Fig. 3. Types of the proposed compliant joints with dimensions

Table I illustrates four mechanisms resulting from the integration of these flexures.

- Model 1 integrates circular joint A with split tube joint C.
- Model 2 integrates the semi-circular undercut joint B with the split tube joint C.
- Model 3 integrates circular joint A with cruciform joint D.
- Model 4 integrates the semi-circular undercut joint B with the cruciform joint D.

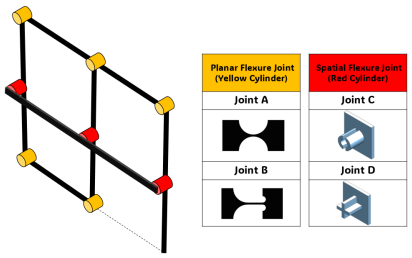


Fig. 4. RCM mechanism with the proposed types of flexure joints

TABLE I. THE PROPOSED RCM MODEL AS A COMBINATION OF THE PROPOSED FLEXURE JOINTS

| | Joint A | Joint B |
|---|---|---|
| Joint C | Model 1 | Model 2 |
| Joint D | Model 3 | Model 4 |

## B. Kinematic Analysis

A kinematic analysis of the RCM tilting mechanism establishes itself based on considering its structure. Fig. 5 illustrates the geometry of the parallel six-bar tilting mechanism as follows: The linear variable input displacement is donated by $X_i$ which represented by the distance between point $B$ and point $C$, The input angle is variable $\angle BAB^{'}$ is donated by $\theta_i$, and the input angle $\theta_i$ equals the output angle $\theta_o$.

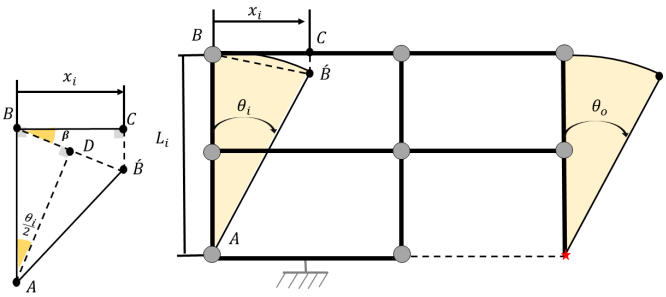


Fig. 5. The geometry of the RCM mechanism

This analysis aims to find a relation between input displacement $X_i$ and the output tilting angle $\theta_o$ .
In $\triangle BCB^{'}$
$BC \perp AB$ then,

$$cos(\beta) = \left(\frac{BC}{BB'}\right) \tag{1}$$

In $\triangle BB^{'}A$
$AB$=$AB^{'}$ & $BD$=$DB^{'}$
Then, $AD \perp BB^{'}$ & $\angle BAD$ =$\angle DAB^{'}$ = $\theta_i/2$

AS $\angle DBA + \theta_i/2 = 90$ & $\angle DBA + \angle DBC\ (\beta) = 90$
Then $\angle\theta_i/2 = \angle DBC\ (\beta)$
For Eq. 1 Replace $\beta$ with $\theta_i/2$ and rewrite Eq. (1)

$$BB^{'} = \left(\frac{BC}{cos(\theta_i/2)}\right) \tag{2}$$

In $\triangle BDA$

$$sin(\theta_i/2) = \left(\frac{BD}{AB}\right) \tag{3}$$

Where $BD$ equals $BB^{'}/2$, Rewrite Eq. 3

$$BB^{'} = 2 * AB * sin(\theta_i/2) \tag{4}$$

From Eq. (2) and Eq. (4)

$$\left(\frac{BC}{cos(\theta_i/2)}\right) = 2 * AB * sin(\theta_i/2) \tag{5}$$

Rearrange Eq. (5)

$$\left(\frac{BC}{AB}\right) = 2 * sin(\theta_i/2) * cos(\theta_i/2) \tag{6}$$

For any angle i.e $\gamma$

$$sin(2\gamma) = 2 * sin(\gamma) * cos(\gamma) \tag{7}$$

Using Eq. (7) and substituting in Eq. (6)

$$sin(\theta_i) = \left(\frac{BC}{AB}\right) \tag{8}$$

Where $BC = X_i$ & $AB = L_i$
Then,

$$\theta_i = sin^{-1}\left(\frac{X_i}{L_i}\right) \tag{9}$$

Where $\theta_i = \theta_o$ Then,

$$\theta_o = sin^{-1}\left(\frac{X_i}{L_i}\right) \tag{10}$$

Equation (10) provides a relation between the input displacement $X_i$ and output tilting angle $\theta_o$.

### C. Finite Element Analysis

We investigated the performance of the proposed compliant mechanisms using finite element method (FEM) analysis. The simulation was conducted using ANSYS software and involved four CAD models, which were generated in SolidWorks and subsequently exported to ANSYS. The CAD models have dimensions of 130 mm by 90 mm, with links measuring 10 mm in width and spatial flexure joints of 5 mm in width as shown in Fig. 6. The Finite Element Analysis (FEA) process starting with the importing for a CAD model from SolidWorks in STEP file format. Subsequently, the engineering data for the PLA material properties is specified as follows: Density: 1.24 g/cm³ - Tensile Yield Strength: 45 MPa - Young's Modulus: 3600 MPa - Poisson's Ratio: 0.35 [69].

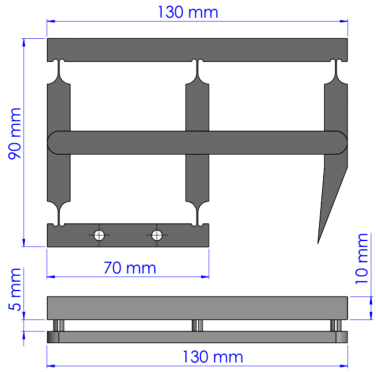


Fig. 6. The proposed CAD model with dimension

Following the definition of material properties, a mesh is created for the model with an element size of 10 mm utilising adaptive sizing. Thereafter, boundary conditions are established as follows: - A: Fixed support - B: Input displacement The objective is to accomplish an output tilting angle of ±30 degrees at the RCM point, as depicted in Fig 7.

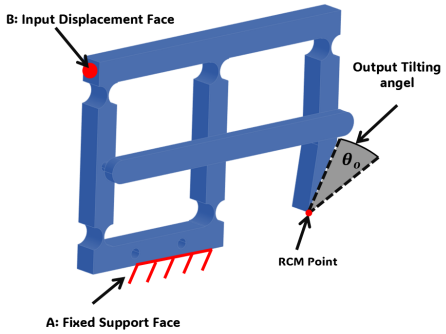


Fig. 7. The exported CAD model with boundary conditions and output measurement

A displacement analysis was performed on the proposed models, as illustrated in Fig. 8. To obtain the results, we first determined the pivot point and then measured the point drift both before and after the motion. An experiment was conducted with displacement inputs in the ±x direction, followed by a tilting angle of the end effector set to ±30°. Fig. 9 shows the relationship between the input displacement in the x direction and the corresponding total RCM (Remote Center of Motion) drifting values for the tested models.

At a tilting angle of ±30°, we assessed deflection along both the x and y axes in order to select the best-performing model, as demonstrated in Fig. 10 and Fig. 11. According to the finite element analysis output data, Model 2 outperformed the others. For instance, at a tilting angle of ±30°, it exhibited minimal drift at the RCM point on both the X and Y axes, with drift measurements of 0.97 mm along the X axis and -2.6453 mm along the Y axis.

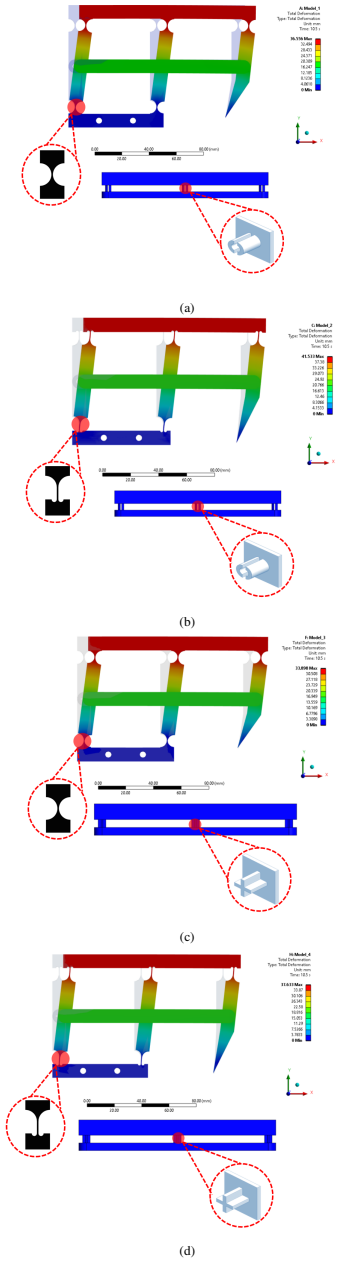


Fig. 8. The proposed RCM Mechanism's displacement analysis for (a) Model 1, (b) Model 2, (c) Model 3 and (d) Model 4

We compared the kinematic analysis equations with the finite element analysis to correlate the input displacement in the x direction with the output tilting angle. Fig. 12 illustrates the results of this comparison.

The modal method is used to analyze the dynamic characteristics of the proposed compliant mechanism [58]. After building the prototype for a high-performance, high-performance RCM-compliant mechanism regarding RCM point drift (Model 2) using SolidWorks, we test it using ANSYS software. The analysis considers the first three natural frequencies, and Fig. 13 shows the mode forms at $f_1 = 52.551$ Hz, $f_2 = 64.428$ Hz and $f_3 = 115.62$ Hz, which correspond to the first three natural frequencies.

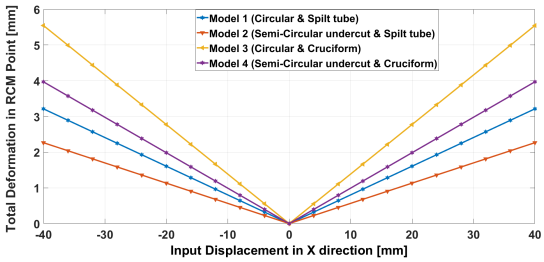


Fig. 9. The input displacement at x direction and total RCM point drift for the suggested models

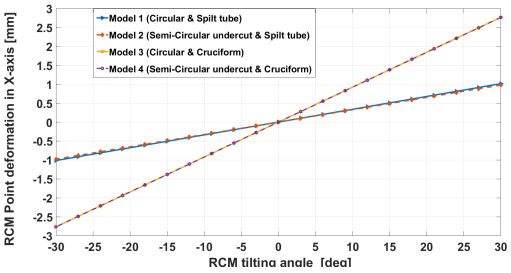


Fig. 10. The x-axis RCM point drift and the output tilting angle for the suggested models

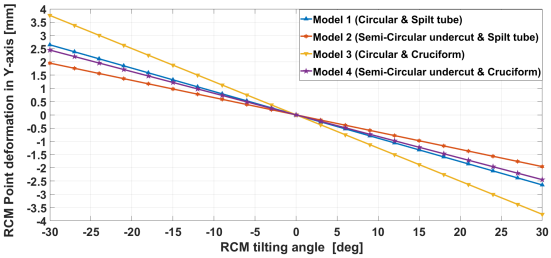


Fig. 11. The y-axis RCM point drift and the output tilting angle for the suggested models

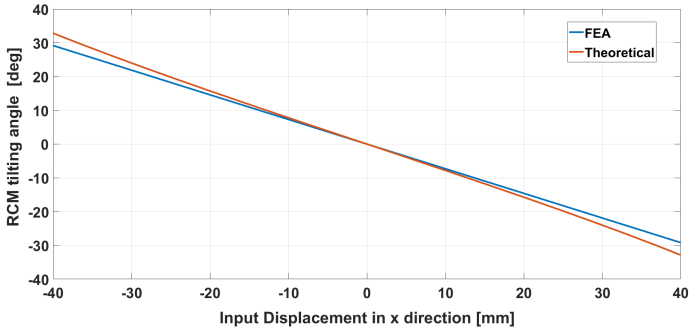


Fig. 12. The relation between input displacement at x direction and output tilting angle.

Examining the RCM mechanism's lowest natural frequency provides valuable insight into its dynamic performances. The first mode value, shown in Fig. 13d, is 52.551 Hz lower than the other five modes, which helps construct the controller for the suggested mechanism with high frequencies.

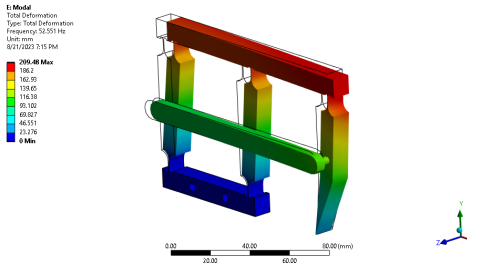

(a) $1^{st}$Mode @31.235

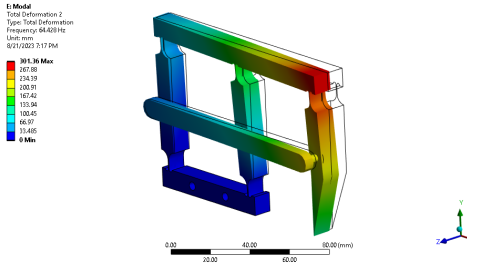

(b) $2^{nd}$Mode @214 Hz

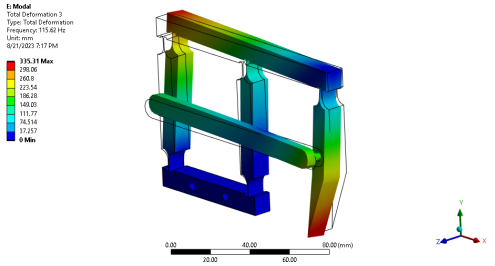

(c) $3^{rd}$ Mode @215.37 Hz

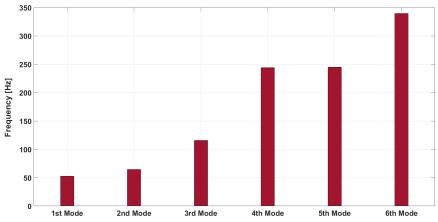


(d) Frequency for the first six modes

Fig. 13. Modal analysis for the proposed mechanism

### *D. Workspace Analysis*

Simulation and validation are carried out in this sub-section for the compliant RCM mechanism. The model is exported to MSC-ADAMS® to establish the nonlinear dynamic model and validate the motion of rolling and tilting with the determination of the workspace and its' boundary. Modelling of the compliant mechanism was established based on the Pseudo-Rigid-Body Model (PRBM ), where each compliant joint is replaced by a revolute joint and torsional spring [59], [60], [70]. We form the workspace by combining rolling and tilting angles in the end-effector trajectories for the desired application. We validate end-effector routes for workspace boundaries to ensure that one input maintains its maximum or minimum value for rolling and tilting inputs. In contrast, the other input actuates throughout its range. The path of end-effector routes from the appropriate workspace is illustrated in Fig. 14.

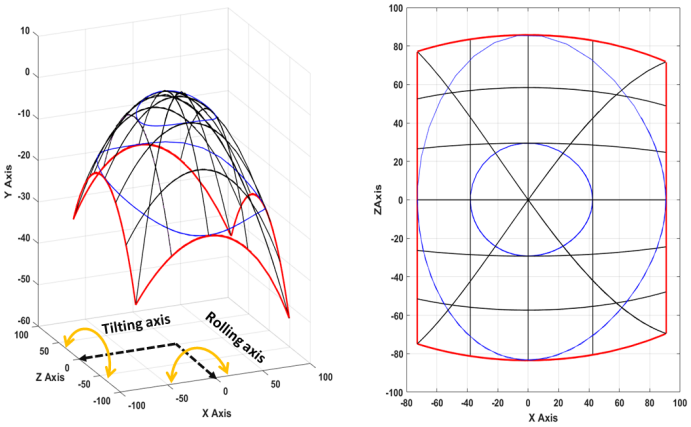


Fig. 14. 2D and 3D graphs for different trajectories of the end-effector

## III. Experiments and Results

This section outlines the validation process for the proposed system. The performance was experimentally evaluated using a prototype of the compliant RCM mechanism to verify the effectiveness of the design. The experimental validation was carried out to assess the mechanism presenting the best results, as outlined in the previous section. The experimental setup is employed to validate the Finite Element Analysis (FEA) results regarding the tilting angle range and RCM point drift. Fig. 15 illustrates the schematic of the complete strategy for design, analysis, and verification.

The fabrication process started with the transfer of a stereolithography file (STL) from SOLIDWORKS to the slicing software. Prusa Slicer 2.9.1 was utilized to adjust the printing parameters and slice the 3D model. The setup utilized PLA material with settings of 100% infill, a printing temperature of 200 °C, a layer height of 0.2 mm, and a print speed of 30 mm/s. Prusa Slicer produced the G-Code, allowing direct printing with the Anycubic Kobra 3D printer.

Fig. 16 illustrates the experimental setup and its components. A linear micrometer (1) is positioned adjacent to the 3D-printed RCM mechanism (2) to adjust the input displacement. An aluminum profile frame (3) mounts an A8-USB digital

microscope (4). Prior to starting the measurement process, the digital microscope requires calibration.

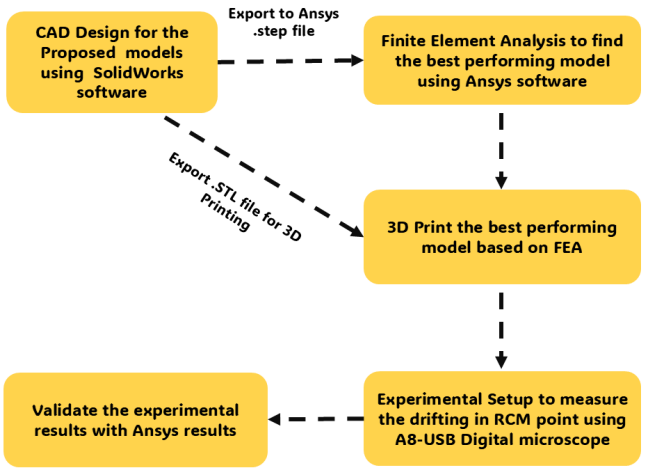


Fig. 15. Schematic for steps of design, analysis and verification processes.

The calibration procedure initiates by connecting the microscope to the computer, followed by the placement of a calibration ruler under the lens. Subsequently, modify the focus and magnification to obtain a clear image of the ruler markings at the specified magnification level. It is essential to maintain the current magnification and focus following this step. Next, access the ”Calibration” feature within the microscope software. Utilise the software’s tool to draw a line across a specified distance on the ruler image, such as exactly 1 mm, to measure a known length. Enter the precise length of the drawn line into the software (e.g., input ”1” and select ”mm”). Finally, save these calibration data.

The experimental setup replicates the FEA simulation process, whereby the micrometer applies input displacement to the RCM mechanism, while the digital microscope evaluates the corresponding tilting angle and RCM point drift. Measurements of the RCM point drift along the x-axis and y-axis at various output tilting angles are carried out as illustrated in Fig. 17. Fig. 18a and Fig. 18b present a comparison of the finite element analysis (FEA) results and experimental data regarding the tilting angle, with the RCM point drifting along the X and Y axes.

## IV. Conclusion

We designed a novel compliant RCM mechanism to streamline integration with a robotic system for micro-surgical applications. The recommended compliant mechanism is better suited for the surgical setting than the mechanical design, which presents challenges such as friction, lubrication, and sterilizing.

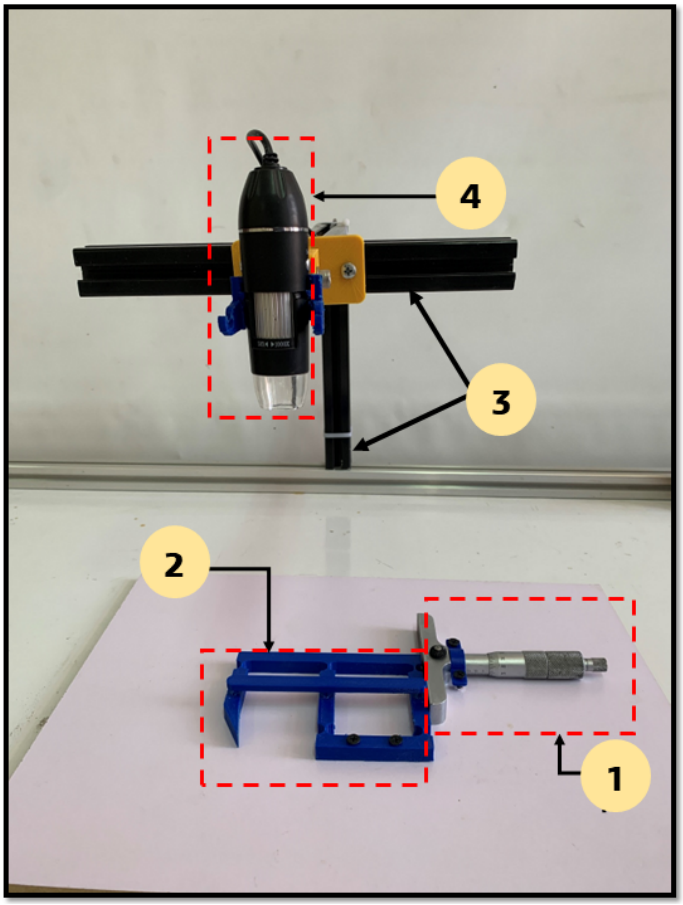


Fig. 16. The measurement Set-up

We assessed the performance of the suggested compliant mechanism using Finite Element Analysis (FEA) software. We then created a prototype of the suggested system and measured the RCM point drift. The experimental measurements deviate slightly from the simulation results, resulting in a maximum displacement of 1.02 mm along the x-axis and 2.07 mm along the y-axis. The most significant difference between the measured and simulated values is 0.056 mm along the x-axis and 0.073 mm along the y-axis.

Future studies should focus on optimising the design and topology of joint shapes to enhance the performance of compliant mechanisms. The laminar jamming approach can be employed in joint design to adjust the stiffness of flexure joints and is integrated with a feedback sensor that evaluates RCM drift. Moreover, advanced control algorithms are utilised for the analysis of force, motion, and joint stiffness.

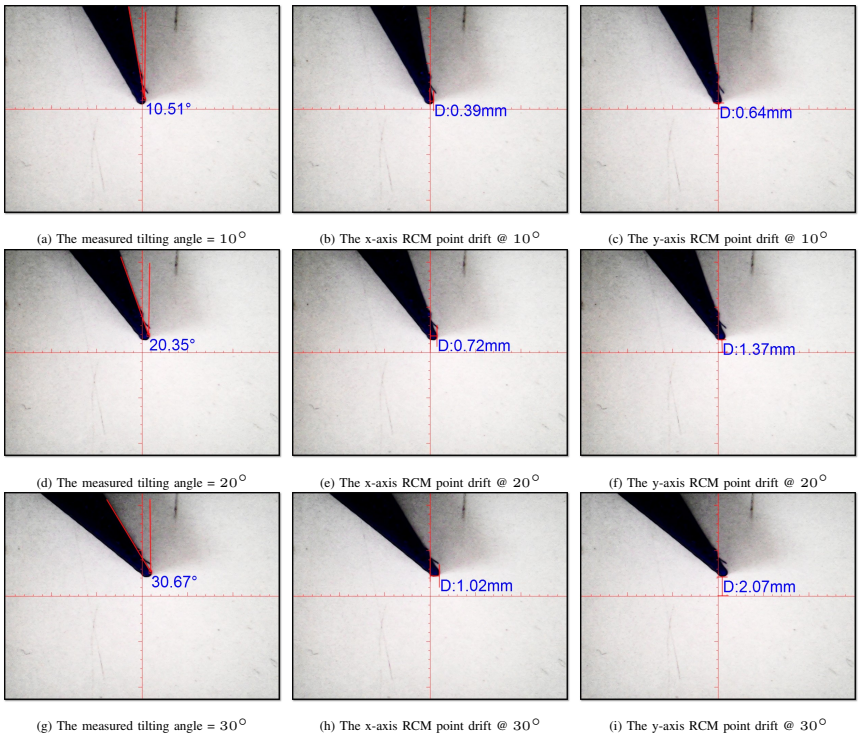


(a) The measured tilting angle = 10° (b) The x-axis RCM point drift @ 10° (c) The y-axis RCM point drift @ 10°

(d) The measured tilting angle = 20° (e) The x-axis RCM point drift @ 20° (f) The y-axis RCM point drift @ 20°

(g) The measured tilting angle = 30° (h) The x-axis RCM point drift @ 30° (i) The y-axis RCM point drift @ 30°

Fig. 17. Measurement output for tilting angle,RCM point drift across X axis and RCM point drift across Y axis

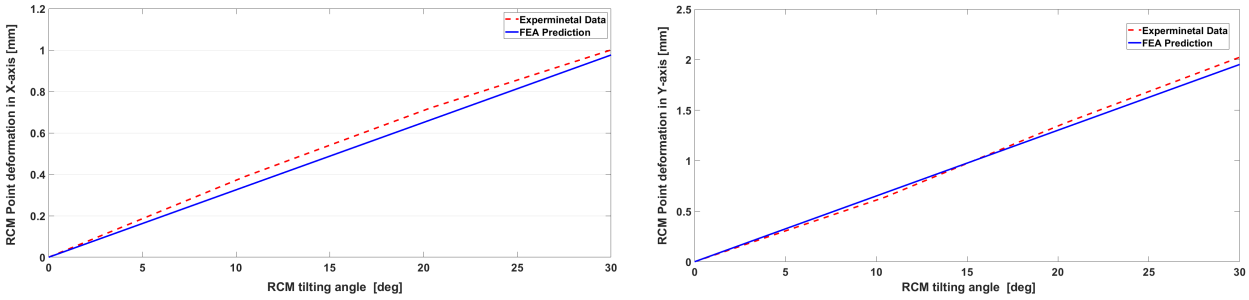


(a) RCM drift across X-axis (b) RCM drift across Y-axis

Fig. 18. Comparison between experimental results and FEA for RCM point drift

## REFERENCES

[1] V. Intriago, M. A. Reina, A. P. Boezaart, R. S. Tubbs, A. V. Montaña, F. J. Pérez-Rodríguez, and M. Sanroman-Junquera, "Microscopy of structures surrounding typical acupoints used in clinical practice and electron microscopic evaluation of acupuncture needles," *Clinical Anatomy*, vol. 35, no. 3, pp. 392–403, 2022, doi: 10.1002/ca.23845.

[2] O. M. Omisore, S. Han, J. Xiong, H. Li, Z. Li and L. Wang, "A Review on Flexible Robotic Systems for Minimally Invasive Surgery," in *IEEE Transactions on Systems, Man, and Cybernetics: Systems*, vol. 52, no. 1, pp. 631-644, 2022, doi: 10.1109/TSMC.2020.3026174.

[3] X. Long, J. Chen, J. Li, and Z. Luo, "The current status and global trends of clinical trials related to robotic surgery: a bibliometric and visualized study," *Journal of Robotic Surgery*, vol. 18, no. 1, pp. 1–12, 2024, doi: 10.1007/s11701-024-01940-8.

[4] R. Chen, P. Rodrigues Armijo, C. Krause, S. R. T. Force, K.-C. Siu, and D. Oleynikov, "A comprehensive review of robotic surgery curriculum and training for residents, fellows, and postgraduate surgical education," *Surgical endoscopy*, vol. 34, pp. 361–367, 2020, doi: 10.1007/s00464-019-06775-1.

[5] R. S. Wang and S. N. Ambani, "Robotic surgery training: current trends and future directions," *Urologic Clinics*, vol. 48, no. 1, pp. 137–146, 2021.

[6] B. Johansson, E. Eriksson, N. Berglund, and I. Lindgren, "Robotic surgery: review on minimally invasive techniques," *Fusion of Multidisciplinary Research, An International Journal*, vol. 2, no. 2, pp. 201–210, 2021.

[7] T. Li, A. Badre, F. Alambeigi, and M. Tavakoli, "Robotic systems and navigation techniques in orthopedics: A historical review," *Applied Sciences*, vol. 13, no. 17, 2023, doi: 10.3390/app13179768.

[8] S. Patel, M. M. Rovers, M. J. Sedelaar, P. L. Zusterzeel, A. F. Verhagen, C. Rosman, and J. P. Grutters, "How can robot-assisted surgery provide value for money?" *BMJ Surgery, Interventions, & Health Technologies*, vol. 3, no. 1, 2021, doi: 10.1136/bmjsit-2020-000042.

[9] T. Fujita, T. Kakuta, N. Kawamoto, Y. Shimahara, S. Yajima, N. Tadokoro, S. Kitamura, J. Kobayashi, and S. Fukushima, "Benefits of robotically-assisted surgery for complex mitral valve repair," *Interactive CardioVascular and Thoracic Surgery*, vol. 32, no. 3, pp. 417–425, 2021, doi:

10.1093/icvts/ivaa271.

[10] D. Pantalone *et al*., "Robot-assisted surgery in space: pros and cons. a review from the surgeon's point of view," *npj Microgravity*, vol. 7, no. 1, 2021, doi: 10.1038/s41526-021-00183-3.

[11] L. Lawrie, K. Gillies, E. Duncan, L. Davies, D. Beard, and M. K. Campbell, "Barriers and enablers to the effective implementation of robotic assisted surgery," *Plos one*, vol. 17, no. 8, 2022, doi: 10.1371/journal.pone.0273696.

[12] J. Spiegelberg, T. Iken, M. K. Diener, and S. Fichtner-Feigl, "Robotic-assisted surgery for primary hepatobiliary tumors—possibilities and limitations," *Cancers*, vol. 14, no. 2, 2022, doi: 10.3390/cancers14020265.

[13] G. Rosiello *et al*., "Partial nephrectomy in frail patients: Benefits of robot-assisted surgery," *Surgical Oncology*, vol. 38, 2021, doi: 10.1016/j.suronc.2021.101588.

[14] A. Mehta, J. C. Ng, W. A. Awuah, H. Huang, J. Kalmanovich, A. Agrawal, T. Abdul-Rahman, M. M. Hasan, V. Sikora, and A. Isik, "Embracing robotic surgery in low-and middle-income countries: Potential benefits, challenges, and scope in the future," *Annals of Medicine and Surgery*, vol. 84, 2022, doi: 10.1016/j.amsu.2022.104803.

[15] F. Struebing, E. Gazyakan, A. Bigdeli, F. Vollbach, J. Weigel, U. Kneser, and A. Boecker, "Implementation strategies and ergonomic factors in robot-assisted microsurgery," *Journal of Robotic Surgery*, vol. 19, no. 1, pp. 1–8, 2025, doi: 10.1007/s11701-024-02199-9.

[16] F. Luo, Y. Xie, J. Yang, H. Yan, X. Chen, G. Cheng, L. Jia, and Q. He, "Improved positioning in robotic assisted laparoscopic partial nephrectomy using the edge mp1000 surgical robot," *Journal of Robotic Surgery*, vol. 19, no. 52, 2025, doi: 10.1007/s11701-024-02183-3.

[17] K. P. Nyein and C. Condron, "Communication and contextual factors in robotic-assisted surgical teams: Protocol for developing a taxonomy," *JMIR Research Protocols*, vol. 13, no. 1, 2024, doi: 10.2196/54910.

[18] A. Agrawal, R. Soni, D. Gupta, and G. Dubey, "The role of robotics in medical science: Advancements, applications, and future directions," *Journal of Autonomous Intelligence*, vol. 7, no. 3, 2024, doi: 10.32629/jai.v7i3.1008.

[19] S. Marcos-Pablos and F. J. García-Peñalvo, "More than surgical tools: a systematic review of robots as didactic tools for the education of professionals in health sciences," *Advances in Health Sciences Education*, vol. 27, no. 4, pp. 1139–1176, 2022, doi: 10.1007/s10459-022-10118-6.

[20] T. Haidegger, S. Speidel, D. Stoyanov and R. M. Satava, "Robot-Assisted Minimally Invasive Surgery—Surgical Robotics in the Data Age," in *Proceedings of the IEEE*, vol. 110, no. 7, pp. 835-846, 2022, doi: 10.1109/JPROC.2022.3180350.

[21] X. Li *et al*., "Robot-assisted partial nephrectomy with the newly developed kangduo surgical robot versus the da vinci si surgical system: a double-center prospective randomized controlled noninferiority trial," *European Urology Focus*, vol. 9, no. 1, pp. 133–140, 2023, doi: 10.1016/j.euf.2022.07.008.

[22] Y. J. Choi, N. T. Sang, H.-S. Jo, D.-S. Kim, and Y.-D. Yu, "A single-center experience of over 300 cases of single-incision robotic cholecystectomy comparing the da vinci sp with the si/xi systems," *Scientific Reports*, vol. 13, no. 1, 2023, doi: 10.1038/s41598-023-36055-x.

[23] O. M. Omisore, S. Han, Y. Al-Handarish, W. Du, W. Duan, T. O. Akinyemi, and L. Wang, "Motion and trajectory constraints control modeling for flexible surgical robotic systems," *Micromachines*, vol. 11, no. 4, 2020, doi: 10.3390/mi11040386.

[24] M. J. Musa, A. B. Carpenter, C. Kellner, D. Sigounas, I. Godage, S. Sengupta, C. Oluigbo, K. Cleary, and Y. Chen, "Minimally invasive intracerebral hemorrhage evacuation: a review," *Annals of biomedical engineering*, vol. 50, no. 4, pp. 365–386, 2022, doi: 10.1007/s10439-022-02934-z.

[25] M. Bai, M. Zhang, H. Zhang, L. Pang, J. Zhao and C. Gao, "An Error Compensation Method for Surgical Robot Based on RCM Mechanism," in *IEEE Access*, vol. 9, pp. 140747-140758, 2021, doi: 10.1109/ACCESS.2021.3117350.

[26] H. Shi, Z. Liang, B. Zhang, and H. Wang, "Design and performance verification of a novel rcm mechanism for a minimally invasive surgical robot," *Sensors*, vol. 23, no. 4, 2023, doi: 10.3390/s23042361.

[27] C. Yan, M. Liu, G. Shi, J. Fan, Y. Li, S. Wu, and J. Hu, "Design of a subretinal injection robot based on the rcm mechanism," *Micromachines*, vol. 14, no. 11, 2023, doi: 10.3390/mi14111998.

[28] A. Singh and J. P. Khatait, "Rcm adjustment for a double-parallelogram based rcm mechanism used for mis robots," *Proceedings of the Institution of Mechanical Engineers, Part C: Journal of Mechanical Engineering Science*, vol. 238, no. 6, pp. 2267–2282, 2024, doi: 10.1177/09544062231185518.

[29] T. Kastritsi and Z. Doulgeri, "A Controller to Impose a RCM for Hands-on Robotic-Assisted Minimally Invasive Surgery," in *IEEE Transactions on Medical Robotics and Bionics*, vol. 3, no. 2, pp. 392-401, 2021, doi: 10.1109/TMRB.2021.3077319.

[30] G. Jeong and S. Y. Ko, "A Novel Vitreoretinal Surgical Robot System to Maximize the Internal Reachable Workspace and Minimize the External Link Motion*," *2024 IEEE/RSJ International Conference on Intelligent Robots and Systems (IROS)*, pp. 4084-4089, 2024, doi: 10.1109/IROS58592.2024.10801874.

[31] W. Zhang, Z. Wang, K. Ma, F. Liu, P. Cheng, and X. Ding, "State of the art in movement around a remote point: a review of remote center of motion in robotics," *Frontiers of Mechanical Engineering*, vol. 19, no. 14, 2024, doi: 10.1007/s11465-024-0785-3.

[32] B. A. Susanto, N. Aurelie, W. Nathaniel, P. Atmodiwirjo, M. R. Ramadan, and R. Djohan, "Conventional and robot-assisted microvascular anastomosis: Systematic review," *Journal of Reconstructive Microsurgery Open*, vol. 9, no. 01, pp. e27–e33, 2024, doi: 10.1055/a-2239-5212.

[33] Y. Rivero-Moreno *et al.*, "Robotic surgery: a comprehensive review of the literature and current trends," *Cureus*, vol. 15, no. 7, 2023, doi: 10.7759/cureus.42370.

[34] G. Malzone, G. Menichini, M. Innocenti, and A. Ballestín, "Microsurgical robotic system enables the performance of microvascular anastomoses: a randomized in vivo preclinical trial," *Scientific Reports*, vol. 13, no. 1, 2023, doi: 10.1038/s41598-023-41143-z.

[35] D. Cannizzaro, M. Scalise, C. Zancanella, S. Paulli, S. Peron, and R. Stefini, "Comparative evaluation of major robotic systems in microanastomosis procedures: A systematic review of current capabilities and future potential," *Brain Sciences*, vol. 14, no. 12, 2024, doi: 10.3390/brainsci14121235.

[36] S. Oh, N. Bae, H.-W. Cho, Y. J. Park, Y. J. Kim, and J.-H. Shin, "Learning curves and perioperative outcomes of single-incision robotic sacrocolpopexy on two different da vinci® surgical systems," *Journal of Robotic Surgery*, vol. 17, no. 4, pp. 1457–1462, 2023, doi: 10.1007/s11701-023-01541-x.

[37] N. Le Chau, N. T. Tran, and T.-P. Dao, "An optimal design method for compliant mechanisms," *Mathematical Problems in Engineering*, vol. 2021, no. 1, 2021, doi: 10.1155/2021/5599624.

[38] G. Mackertich-Sengerdy, S. D. Campbell, and D. H. Werner, "Tailored compliant mechanisms for reconfigurable electromagnetic devices," *Nature communications*, vol. 14, no. 1, 2023, doi: 10.1038/s41467-023-36143-6.

[39] J. Zhan, Y. Li, Z. Luo, and M. Liu, "Topological design of multi-material compliant mechanisms with global stress constraints," *Micromachines*, vol. 12, no. 11, 2021, doi: 10.3390/mi12111379.

[40] M. Kabganian and S. M. Hashemi, "Towards design optimization of compliant mechanisms: A hybrid pseudo-rigid-body model–finite element method approach and an accurate empirical compliance equation for circular flexure hinges," *Biomimetics*, vol. 9, no. 8, 2024, doi: 10.3390/biomimetics9080471.

[41] P. K. Jambhale and B. B. Deshmukh, "Application of compliant mechanisms in various fields—a review," in *Biennial International Conference on Future Learning Aspects of Mechanical Engineering*, pp. 707–716, 2023, doi: 10.1007/978-981-99-3033-3_58.

[42] M. P. Dang, H. G. Le, N. T. D. Tran, N. L. Chau, and T.-P. Dao, "Optimal design and analysis for a new 1-dof compliant stage based on additive manufacturing method for testing medical specimens," *Symmetry*, vol. 14, no. 6, 2022, doi: 10.3390/sym14061234.

[43] Z. Zhang, M. Pieber, and J. Gerstmayr, "Generalized optimization approach to design in-plane distributed compliant remote center of motion mechanism," *Mechanism and Machine Theory*, vol. 205, 2025, doi: 10.1016/j.mechmachtheory.2024.105890.

[44] R. Chen, L. Liu, L. Zhou, R. Cheng, W. Wang, K. Wu, R. Li, X. Li, and G. Zheng, "Design and optimization of a planar anti-buckling compliant rotational joint with a remote center of motion," *Mechanism and Machine Theory*, vol. 203, 2024, doi: 10.1016/j.mechmachtheory.2024.105816.

[45] K. Chandrasekaran, A. Somayaji, and A. Thondiyath, "Realization of a statically balanced compliant planar remote center of motion mechanism for robotic surgery," in *2018 Design of Medical Devices Conference*, 2018, doi: 10.1115/DMD2018-6911.

[46] M. Gaafar, M. Magdy, A. T. Elgammal, A. El-Betar and A. M. Saeed, "Development of a New Compliant Remote Center of Motion (RCM) Mechanism for Vitreoretinal Surgery," *2020 6th International Conference on Control, Automation and Robotics (ICCAR)*, pp. 183-187, 2020, doi: 10.1109/ICCAR49639.2020.9108005.

[47] Y. Li, S. Wu, J. Fan, T. Jiang, and G. Shi, "Design and analysis of a spatial 2r1t remote center of motion mechanism for a subretinal surgical robot," in *Actuators*, vol. 13, no. 4, 2024, doi: 10.3390/act13040124.

[48] X. Zhao, F. Wang, C. Tao, B. Shi, Z. Huo, and Y. Tian, "Development of a novel retinal surgery robot based on spatial variable remote center-of-motion mechanism," *Journal of Mechanisms and Robotics*, vol. 17, no. 3, 2025, doi: 10.1115/1.4066135.

[49] J. Qiu, J. Wu, and B. Zhu, "Optimization design of a parallel surgical robot with remote center of motion," *Mechanism and Machine Theory*, vol. 185, 2023, doi: 10.1016/j.mechmachtheory.2023.105327.

[50] T. Huo, J. Yu, H. Zhao, H. Wu, and Y. Zhang, "A family of novel rcm rotational compliant mechanisms based on parasitic motion compensation," *Mechanism and Machine Theory*, vol. 156, 2021, doi: 10.1016/j.mechmachtheory.2020.104168.

[51] Z. Wang, W. Zhang, and X. Ding, "A family of rcm mechanisms: type synthesis and kinematics analysis," *International Journal of Mechanical Sciences*, vol. 231, 2022, doi: 10.1016/j.ijmecsci.2022.107590.

[52] A. Antonov, "Parallel–serial robotic manipulators: a review of architectures, applications, and methods of design and analysis," *Machines*, vol. 12, no. 11, 2024, doi: 10.20944/preprints202410.1906.v1.

[53] X. Lv, F. Ye, K. Wang, H. Sun, and Y. Cao, "A new family of double-stage parallel mechanisms with movable rcm," *Robotica*, pp. 1–24, 2024, doi: 10.1017/S0263574724002108.

[54] S. Aksungur, M. Aydin, and O. Yakut, "Real-time pid control of a novel rcm mechanism designed and manufactured for use in laparoscopic surgery," *Industrial Robot: the international journal of robotics research and application*, vol. 47, no. 2, pp. 153–166, 2020, doi: 10.1108/IR-09-2019-0179.

[55] Y. Yang, H. Liu, H. Zheng, Y. Peng, and Y. Yu, "Two types of remote-center-of-motion deployable manipulators with dual scissor-like mechanisms," *Mechanism and Machine Theory*, vol. 160, 2021, doi: 10.1016/j.mechmachtheory.2021.104274.

[56] M. Sattari Sarebangholi and F. Najafi, "Design of a path generating compliant mechanism using a novel rigid-body-replacement method," *Meccanica*, vol. 57, no. 7, pp. 1701–1711, 2022, doi: 10.1007/s11012-022-01527-3.

[57] S. Liao, B. Ding, and Y. Li, "Design, assembly, and simulation of flexure-based modular micro-positioning stages," *Machines*, vol. 10, no. 6, 2022, doi: 10.3390/machines10060421.

[58] D. D. Baviskar, A. Rao, S. Sollapur, and P. P. Raut, "Development and testing of xy stage compliant mechanism," *International Journal on Interactive Design and Manufacturing (IJIDeM)*, vol. 18, no. 7, pp. 5197–5210, 2024, doi: 10.1007/s12008-023-01612-1.

[59] Y. Hahnemann, M. Weiss, M. Bernek, I. Boblan, and S. Götz, "Advancing biomechanical simulations: A novel pseudo-rigid-body model for flexible beam analysis," *Biomechanics*, vol. 4, no. 3, pp. 566–584, 2024, doi: 10.3390/biomechanics4030040.

[60] M. Magdy and M. Gaafar, "Design and Analysis of a New Compliant Gripper for Microgripper Applications," *2023 4th International Conference on Artificial Intelligence, Robotics and Control (AIRC)*, pp. 41-45, 2023, doi: 10.1109/AIRC57904.2023.10303209.

[61] K. Dwarshuis, R. Aarts, M. Ellenbroek, and D. Brouwer, "Efficient computation of large deformation of spatial flexure-based mechanisms in design optimizations," *Journal of Mechanisms and Robotics*, vol. 15, no. 2, 2023, doi: 10.1115/1.4054730.

[62] M. Tschiersky, J. J. de Jong, and D. M. Brouwer, "Flexure hinge design and optimization for compact anthropomorphic grippers made via metal additive manufacturing," *Journal of Mechanical Design*, vol. 146, no. 1, 2024, doi: 10.1115/1.4063362.

[63] J. Rommers, V. van der Wijk, and J. L. Herder, "A new type of spherical flexure joint based on tetrahedron elements," *Precision Engineering*, vol. 71, pp. 130–140, 2021, doi: 10.1016/j.precisioneng.2021.03.002.

[64] C. Li, N. Wang, B. Chen, G. Shang, X. Zhang, and W. Chen, "Spatial compliance modeling and optimization of a translational joint using corrugated flexure units," *Mechanism and Machine Theory*, vol. 176, 2022, doi: 10.1016/j.mechmachtheory.2022.104962.

[65] F. Harfensteller, S. Henning, L. Zentner, and S. Husung, "Modeling of corner-filleted flexure hinges under various loads," *Mechanism and Machine Theory*, vol. 175, 2022, doi: 10.1016/j.mechmachtheory.2022.104937.

[66] D. D. Sonneveld, J. Nijssen, and R. A. van Ostayen, "Compliant joints utilizing the principle of closed form pressure balancing," *Journal of Mechanical Design*, vol. 145, no. 8, 2023, doi: 10.1115/1.4062583.

[67] M. Arredondo-Soto, E. Cuan-Urquizo, and A. Gómez-Espinosa, "A review on tailoring stiffness in compliant systems, via removing material: Cellular materials and topology optimization," *Applied Sciences*, vol. 11, no. 8, 2021, doi: 10.3390/app11083538.

[68] P. Kuresangsai, M. O. Cole, and G. Hao, "Analysis and design optimization of a compliant robotic gripper mechanism with inverted flexure joints," *Mechanism and Machine Theory*, vol. 202, 2024, doi: 10.1016/j.mechmachtheory.2024.105779.

[69] T. Pepelnjak, A. Karimi, A. Maček, and N. Mole, "Altering the elastic properties of 3d printed poly-lactic acid (pla) parts by compressive cyclic loading," *Materials*, vol. 13, no. 19, 2020, doi: 10.3390/ma13194456.

[70] Vedant and J. T. Allison, "Pseudo-rigid-body dynamic models for design of compliant members," *Journal of Mechanical Design*, vol. 142, no. 3, 2020, doi: 10.1115/1.4045602.